The coherence of superradiance

R. Lopes, A. Imanaliev, M. Bonneau,* J. Ruaudel, M. Cheneau, D. Boiron, and C. I. Westbrook†
Laboratoire Charles Fabry, Institut d'Optique, CNRS, Univ. Paris-Sud, 2 avenue Augustin Fresnel, 91127 Palaiseau, France
(Dated: December 25, 2013)

We have measured the 2nd order coherence, or 2-body correlations, of atoms from a Bose–Einstein condensate participating in a superradiance process. We compare the statistics of the superradiant phenomenon with the ordinary spontaneous emission and with a coherent source obtained via a stimulated Raman transition of a Bose–Einstein condensate. Despite strong stimulated emission the correlation properties of the superradiance are close to those of a thermal sample.

PACS numbers: 03.75.Kk, 67.10.Jn, 42.50.Lc

Ever since the publication of Dicke's 1954 paper [1], the problem of the collective emission of radiation has occupied many researchers in the fields of light scattering, lasers and quantum optics. Originally dubbed superradiance, this process underlies much of the physics of lasers [2] and has been observed in many different contexts: hot gases, cold gases, solids and even planetary and astrophysical environments [3]. Collective emission is characterized by a rate of emission which is strongly modified compared to that of the individual atoms [4]. Research has shown that the details depend on many parameters such as pumping configuration, dephasing and relaxation processes, sample geometry etc. and, as a result, a complex nomenclature has evolved including the terms superradiance, superfluorescence, amplified spontaneous emission, mirrorless lasing, and random lasing [2, 4–8], the distinctions among which we will not attempt to summarize here.

Although collective emission has been studied for at least 60 years, the problem has recently seen renewed interest in the field of cold atoms [9–24]. This is partly because cold atoms provide a reproducible, easily characterized ensemble in which Doppler broadening effects are small and relaxation is generally limited to spontaneous emission. Most cold atom experiments differ in an important way from the archetypal situation first envisioned by Dicke: instead of creating an ensemble of excited atoms at a well defined time and then allowing this ensemble to evolve freely, the sample is typically pumped during a period long compared to the relaxation time and emission lasts essentially only as long as the pumping. The authors of reference [9] however, have argued that there is a close analogy to the Dicke problem, and we will follow them in designating this process as superradiance.

An important method to characterize the emission of radiation consists in considering its coherence properties. The term coherence is often applied to the atomic dipoles which emit the radiation. In this paper however, we use it only for the radiation itself. Thus, coherence allows one to distinguish lasers from other sources such as thermal or chaotic ones [25]. We tend to characterize a laser by its high phase coherence, measured by the 1st order correlation function, and a stable intensity, corresponding to a flat 2nd order correlation function. In the literature on superradiance however, there has been relatively little discussion about the coherence and correlation properties of the light. The theoretical treatments we are aware of show that the coherence of collective emission can be quite complicated and does not resemble that of a laser [4, 12, 19, 26–28]. Experimentally, there has been even less published work, but it corroborates the view that superradiance is not coherent in the sense of laser emission [23, 29].

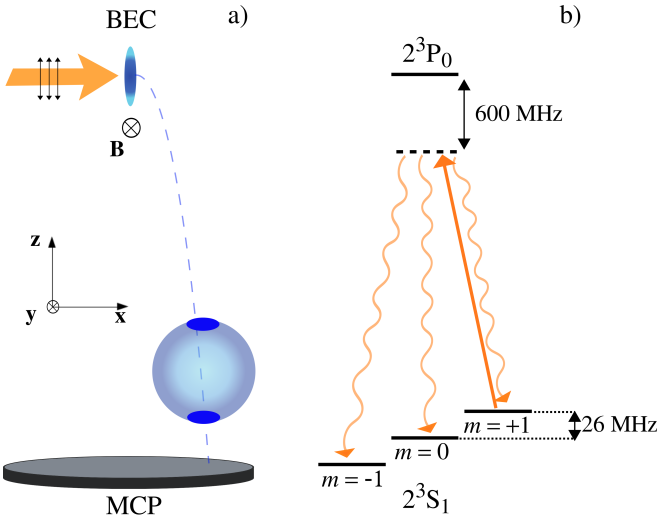

FIG. 1: (color online) a) Sketch of the experiment. A 9-G magnetic field $\mathbf{B}$ applied along the y axis defines the quantization axis. The excitation beam propagates with an angle of 10° (not shown) relative to the x axis and its polarization is linear, with the same angle relative to the y axis. After emission, the atoms fall 46 cm to a position-sensitive micro-channel plate (MCP). The atom cloud forms a sphere with enhanced occupation of the endfire modes. b) Atomic level scheme. The atoms, initially in the 2^3S_1, $m = +1$ state, are excited to the 2^3P_0 state. From there, they can decay with equal branching ratios to the 3 sub-levels of the ground state. We detect only the atoms which scatter into the $m = 0$ state.

In this work we study collective emission of light from atoms in a Bose–Einstein condensate (BEC). Starting from initially nearly motionless atoms, we observe their recoil upon emission. To the extent that each recoil corresponds to the emission of a single photon, we can obtain essentially the same information about the radiation from such measurements as by observing it directly. In doing this, we are following the approach pioneered in experiments such as [9, 29]

and followed by many others, which uses highly developed atom detection and imaging techniques to glean most of the experimental information about the process. We use measurements of individual atomic recoils to construct 2-particle correlation functions (2nd order correlation functions). We are able to make time-integrated measurements of the emission, resolved in transverse and longitudinal momentum as well as in polarization. We will show that in the configuration of our experiment, the 2nd order correlation of the recoiling atoms is close to that of a thermal sample, and very different from the correlation properties of the initial, condensed atomic state.

Our experimental configuration corresponds to "Raman superradiance" [14, 30], by which we mean that an absorption and emission cycle is accompanied by a change of the internal state of the atom. We excite atoms in an elongated BEC in such a way that an allowed emission dipole can radiate along the long axis. In an anisotropic source, collective emission builds up more efficiently in the directions of highest optical thickness. Superradiance is therefore expected to occur along the long axis of the BEC, in so called "endfire" modes [31]. We use helium in the 2^3S_1, $m = +1$ state confined in a crossed dipole trap (see Fig. 1a) with frequencies of 1300 Hz in the x and y directions and 130 Hz in the (vertical) z direction. The dipole trap wavelength is $1.5\,\mu$m. The atom number is approximately 50 000 and the temperature of the remaining thermal cloud is 140 nK. A 9-G magnetic field along the y axis defines a quantization axis.

After producing the condensate, we irradiate it with a laser pulse of 2.4 W/cm^2 tuned 600 MHz to the red of the $2^3S_1 \rightarrow 2^3P_0$ transition at $\lambda = 1083$ nm. The excitation laser propagates in a plane nearly orthogonal to the quantization axis. Its polarization is linear and approximately orthogonal to the quantization axis. The pulse length is $5\,\mu$s and it is applied with a delay τ after switching off the trap. The level scheme is shown in Fig. 1b. The absorption dipole matrix element is of the σ^- form and thus one half of the laser intensity is coupled to the atomic transition corresponding to a Rabi frequency of 56 MHz. The excited atoms decay with equal branching ratios to the 3 ground states. During the pulse, less than 10 % of the atoms are pumped into each of these states. Because of the polarization selection rules, the atoms which are pumped into the $m = 0$ state cannot reabsorb light from the excitation laser. An important parameter in superradiance is the Fresnel number of the sample [4], $F = 2R_\perp^2/\lambda R_z$, where $R_\perp$ and R_z are the horizontal and vertical Thomas–Fermi radii of the condensate. The Fresnel number distinguishes between the diffraction limited ($F < 1$) and multimode superradiance regimes ($F > 1$). In our case, $R_\perp \approx 5\,\mu$m and $R_z \approx 50\,\mu$m, yielding a Fresnel number of about unity.

When the trap is switched off, the atoms fall toward a micro-channel plate detector which detects individual atoms with 3 dimensional imaging capability and a 10 to 20 % quantum efficiency [32]. A magnetic field gradient is applied to sweep away all atoms except those scattered into the $m = 0$ magnetic sublevel. The average time of flight to the detector is 310 ms and is long enough that the atoms' positions at the detector reflect the atomic momenta after interaction with the excitation laser. Conservation of momentum requires that the scattered atoms lie on a sphere with a radius equal to the recoil momentum $k_{\rm rec} = 2\pi/\lambda$.

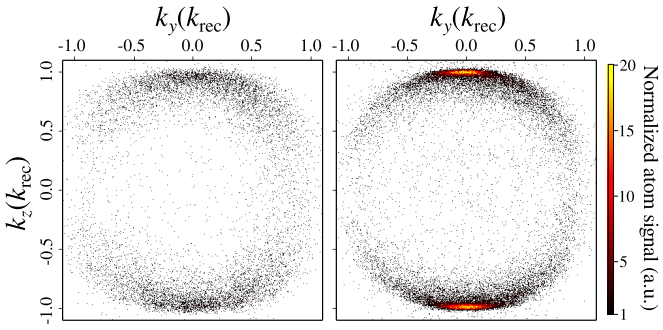

FIG. 2: (color online) Momentum distribution of scattered atoms in the plane of the emission dipole. Both figures show the distribution in the yz plane, integrated between $k_x = \pm 0.1\,k_{\rm rec}$ and summed over 100 shots. Left: Excitation laser applied 500 μs after the trap has been switched off. Only the radiation pattern for a y-polarized dipole is visible. Right: Excitation laser applied immediately after the trap has been switched off. Strong superradiance is visible in the vertical, endfire modes.

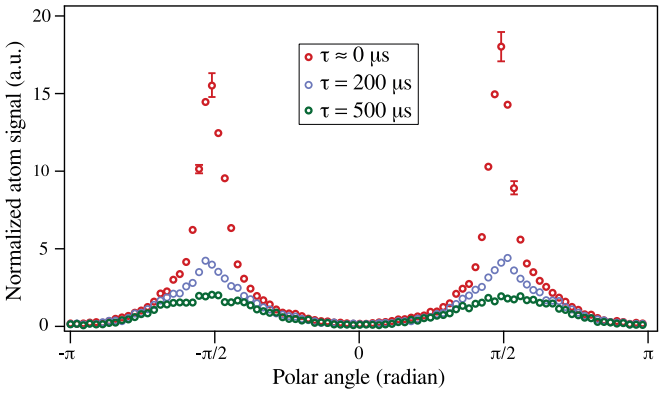

FIG. 3: (color online) Angular distribution of scattered atoms in the plane of the emission dipole for different values of the delay τ before the excitation pulse. The data for $\tau = 0$ and 500 μs are the same as those shown in Fig. 2. The images were integrated along the x axis between $\pm 0.1\,k_{\rm rec}$. The delays $\tau = 0$, 200 and 500 μs correspond to peak densities of $\approx 8,\ 2,\ 0.4 \times 10^{18}\,{\rm m}^{-3}$ and to aspect ratios of 10, 5 and 2.5, respectively. The endfire modes are located at $\pm\pi/2$. The half-width at half-maximum of the highest peak is 0.14 rad. Typical error bars are shown and denote the 68% confidence interval. Away from the endfire modes the error bars would not be visible on that scale.

Typical images are shown in Fig. 2, for $\tau = 500\mu$s (left panel) and $\tau \approx 0$ (right panel). Strong scattering in the endfire modes is evident for the short delay. Moreover, from $\tau = 500\,\mu$s to $\tau \approx 0$, the total number of scattered atoms is increased by a factor of ~ 5. This demonstrates the collective nature of the superradiant emission when the sample is dense and anisotropic. At long delays, the condensate has

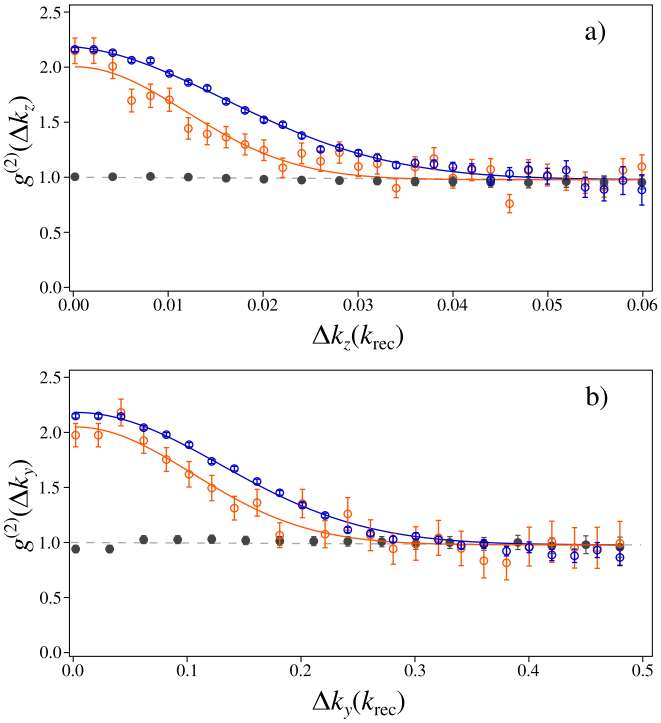

FIG. 4: (color online) Correlation functions along the z (a) and y axis (b) for $\tau \approx 0$. Blue circles correspond to the superradiant peaks (defined by $|k_z| > 0.95k_{\rm rec}$). Orange circles correspond to atoms from the scattering sphere away from the superradiant peaks (defined by $|k_z| < 0.92k_{\rm rec}$). Solid lines are Gaussian fits constrained to approach unity at large separation. Gray solid circles correspond to a fraction of the initial condensate transferred to the $m = 0$ state via a stimulated Raman transfer. The dashed gray line shows unity. Error bars denote the 68% confidence interval.

expanded sufficiently that the optical thickness and anisotropy have fallen dramatically, suppressing the collective scattering. By looking at the number of scattered atoms in the x direction (perpendicular to the plane of Fig. 2), we have verified that, away from the endfire modes, the scattering rate varies by less than 10% for different delays [33].

To see the distribution in a more quantitative way, we show in Fig. 3 an angular plot of the atom distribution in the yz plane. Data is shown for three different delays τ before application of the excitation pulse. The angles 0 and π correspond to the orientation of the emission dipole and thus the scattering rate vanishes. For short delay the half width of the superradiant peaks is $0.14\,k_{\rm rec}$, or 0.14 rad, consistent with the diffraction angle and the aspect ratio of the source. In the vertical direction, the superradiant peaks are 10 times narrower than in the horizontal direction [33]. In the strongly superradiant case, the heights of the two peaks differ slightly. On a shot-to-shot basis we observe even greater fluctuations in this difference and the data shown may partly reflect the imperfect averaging of these fluctuations.

We investigate the coherence of the scattered atoms by measuring the normalized 2nd order correlation function defined as

$$g^{(2)}(\Delta\mathbf{k}) = \frac{\langle :\hat{n}(\mathbf{k})\hat{n}(\mathbf{k}+\Delta\mathbf{k}): \rangle}{\langle \hat{n}(\mathbf{k})\rangle \, \langle \hat{n}(\mathbf{k}+\Delta\mathbf{k})\rangle} \,. \qquad (1)$$

Here $\hat{n}$ is the atomic density and :: denotes normal ordering. The experimental realization of this function consists in a histogram of pair separations as a function of $\Delta\mathbf{k}$ normalized to the autoconvolution of the average particle momentum distribution [34, 35]. Figure 4 shows the experimentally measured correlation function integrated over the momentum along two out of three axes both for the superradiant peaks and on the scattering sphere away from the peaks [33].

We see that in both cases the correlation function at zero separation reaches a value close to 2. For the superradiant peaks, the correlation is even slightly larger than 2, a behavior which has appeared already in calculations [19, 36]. This shows that, despite strong stimulated emission in the endfire modes, the atoms undergoing a superradiant process have statistics consistent with those of a thermal sample. We attribute these large intensity fluctuations to the fact that superradiant emission is triggered by spontaneous emission. This does not prevent the superradiant process to be used as a coherent matter wave amplifier [37, 38] since in this case the process is seeded by a coherent (BEC) pulse.

Figure 4 also shows that the correlation widths of the superradiant peaks are somewhat broader than those of the spontaneously scattered atoms. The effect is a factor of about 1.5 in the vertical direction and about 1.25 in the horizontal direction [33]. The broadening indicates that the effective source size for superradiance is slightly smaller than for spontaneous scattering. A decreased vertical source size for superradiance is consistent with the observations of Ref. [39, 40] which showed that the superradiant emission is concentrated near the ends of the sample. In the horizontal direction, one also expects a slightly reduced source size relative to the atom cloud since the gain is higher in the center. The fact that the correlation widths are close to the widths of the momentum distribution [33] indicates that the superradiant peaks are almost single mode as expected for samples with a Fresnel number close to 1 [4].

The spontaneous superradiant scattering process should be contrasted with stimulated Raman scattering. To characterize the latter, we applied the excitation beam together with another beam polarized parallel to the magnetic field and detuned by the Zeeman shift (26 MHz) with respect to the σ-polarized beam, inducing a stimulated Raman transition. The intensities were adjusted to transfer a similar number of atoms to the $m = 0$ state as in the superradiance experiment. The normalized correlation functions in this situation, shown in Fig. 4, are very nearly flat and equal to unity as we expect for a BEC [34, 41, 42]. The superradiant atom peaks also appear to exhibit a sort of longitudinal gain narrowing effect [27]. We observe them to be 2.8 times narrower in the vertical direction than the vertical width of the transferred condensate [33], but we have not yet made a careful study of this effect.

We also investigated the case when the atomic sample was

excited with a longer and stronger pulse (10 μs, 3.2 W/cm^2), so that the initial condensate was entirely depleted. The correlation function of the superradiant peaks were practically identical to the one measured for a weaker depletion. Finally, we have measured correlation functions for a few other configurations: the Rayleigh scattering regime, in which the atoms scatter back to their initial internal state, and for a trapped BEC with a longitudinal confinement frequency of 7 Hz, leading to a much greater aspect ratio. These configurations also led to approximately thermal correlations.

We emphasize that our observations have been on the atoms undergoing superradiance rather than on the radiation itself. Because each atomic scattering event corresponds to a photon emission, however, we infer that the emitted light should also resemble thermal radiation. Nonetheless the temporal characteristics of the light pulse in the longitudinal direction will be very different from those of the atomic pulse ($\sim$ 300 μs at the detector). The light pulse will have a total duration essentially equal to that of the excitation pulse, although its temporal shape might be complex as shown in Ref. [9]. An interesting extension of the techniques used here is to examine superradiant Rayleigh scattering of a light pulse short enough and strong enough to populate oppositely directed modes [43]. It has been predicted [12, 13, 44] that the modes propagating in opposite direction are entangled, similar to those produced in atomic four wave mixing [45–47]. A similar measurement technique should be able to reveal them.

We acknowledge fruitful discussions with A. Browaeys, J.-J. Greffet and P. Pillet. This work was supported by the IFRAF institute, the Triangle de la Physique, the LABEX PALM, the ANR-ProQuP project, the ERC (Grant No. 267 775) Quantatop, J.R. by the DGA, R.L. by the FCT scholarship SFRH/BD/74352/2010.

* Current address: INO-CNR, viaG. Sansone 1, 50019 Sesto Fiorentino - Firenze, Italy
† Electronic address: christoph.westbrook@institutoptique.fr

[1] R. H. Dicke, Phys. Rev. **93**, 99 (1954).
[2] A. E. Siegman, *Lasers* (University Science Books, Mill Valley, CA, 1986).
[3] V. Letokhov and S. Johansson, *Astrophysical Lasers* (Oxford University Press, 2008).
[4] M. Gross and S. Haroche, Phys. Rep. **93**, 301 (1982).
[5] N. Rehler and J. Eberly, Phys. Rev. A **3**, 1735 (1971).
[6] L. Allen and G. Peters, Phys. Rev. A **8**, 2031 (1973).
[7] R. Bonifacio and L. Lugiato, Phys. Rev. A **11**, 1507 (1975).
[8] J. MacGillivray and M. Feld, Phys. Rev. A **14**, 1169 (1976).
[9] S. Inouye, A. P. Chikkatur, D. M. Stamper-Kurn, J. Stenger, D. E. Pritchard, and W. Ketterle, Science **285**, 571 (1999).
[10] M. G. Moore, O. Zobay, and P. Meystre, Phys. Rev. A **60**, 1491 (1999).
[11] Ö. E. Müstecaplioglu and L. You, Phys. Rev. A **62**, 063615 (2000).
[12] N. Piovella, M. Cola, and R. Bonifacio, Phys. Rev. A **67**, 013817 (2003).
[13] H. Pu, W. Zhang, and P. Meystre, Phys. Rev. Lett. **91**, 150407 (2003).
[14] Y. Yoshikawa, T. Sugiura, Y. Torii, and T. Kuga, Phys. Rev. A **69**, 041603 (2004).
[15] N. Bar-Gill, E. E. Rowen, and N. Davidson, Phys. Rev. A **76**, 043603 (2007).
[16] T. Wang, S. Yelin, R. Côté, E. Eyler, S. Farooqi, P. Gould, M. Koštrun, D. Tong, and D. Vrinceanu, Phys. Rev. A **75**, 033802 (2007).
[17] E. Paradis, B. Barrett, A. Kumarakrishnan, R. Zhang, and G. Raithel, Phys. Rev. A **77**, 043419 (2008).
[18] A. Hilliard, F. Kaminski, R. le Targat, C. Olausson, E. S. Polzik, and J. H. Müller, Phys. Rev. A **78**, 051403 (2008).
[19] D. Meiser and M. J. Holland, Phys. Rev. A **81**, 063827 (2010).
[20] L. Deng, E. W. Hagley, Q. Cao, X. Wang, X. Luo, R. Wang, M. G. Payne, F. Yang, X. Zhou, X. Chen, et al., Phys. Rev. Lett. **105**, 220404 (2010).
[21] T. Vogt, B. Lu, X. Liu, X. Xu, X. Zhou, and X. Chen, Phys. Rev. A **83**, 053603 (2011).
[22] J. G. Bohnet, Z. Chen, J. M. Weiner, D. Meiser, M. J. Holland, and J. K. Thompson, Nature **484**, 78 (2012).
[23] J. A. Greenberg and D. J. Gauthier, Phys. Rev. A **86**, 013823 (2012).
[24] Q. Baudouin, N. Mercadier, V. Guarrera, W. Guerin, and R. Kaiser, Nat. Phys. **9**, 357 (2013).
[25] R. Loudon, *The quantum theory of light* (Oxford University Press, Oxford; New York, 2000).
[26] F. Haake and R. J. Glauber, Phys. Rev. A **5**, 1457 (1972).
[27] M. G. Moore and P. Meystre, Phys. Rev. Lett. **83**, 5202 (1999).
[28] V. V. Temnov and U. Woggon, Opt. Express **17**, 5774 (2009).
[29] J. M. Raimond, P. Goy, M. Gross, C. Fabre, and S. Haroche, Phys. Rev. Lett. **49**, 1924 (1982).
[30] D. Schneble, G. K. Campbell, E. W. Streed, M. Boyd, D. E. Pritchard, and W. Ketterle, Phys. Rev. A **69**, 041601 (2004).
[31] R. H. Dicke, in *Quantum electronics; proceedings of the third international congress, Paris.*, edited by P. Grivet and N. Bloembergen (Columbia University Press, 1964).
[32] J.-C. Jaskula, M. Bonneau, G. B. Partridge, V. Krachmalnicoff, P. Deuar, K. V. Kheruntsyan, A. Aspect, D. Boiron, and C. I. Westbrook, Phys. Rev. Lett. **105**, 190402 (2010).
[33] See supplementary material at http://link.aps.org/supplemental/XXX for the atomic distribution in the xz plane, details on the calculation of the correlation functions and a table summarizing the widths of the momentum distributions and correlation functions.
[34] M. Schellekens, R. Hoppeler, A. Perrin, J. V. Gomes, D. Boiron, A. Aspect, and C. I. Westbrook, Science **310**, 648 (2005).
[35] K. V. Kheruntsyan, J.-C. Jaskula, P. Deuar, M. Bonneau, G. B. Partridge, J. Ruaudel, R. Lopes, D. Boiron, and C. I. Westbrook, Phys. Rev. Lett. **108**, 260401 (2012).
[36] T. Wasak, J. Chwedeńczuk, P. Ziń, and M. Trippenbach, Phys. Rev. A **86**, 043621 (2012).
[37] S. Inouye, T. Pfau, S. Gupta, A. P. Chikkatur, A. Gorlitz, D. E. Pritchard, and W. Ketterle, Nature **402**, 641 (1999).
[38] M. Kozuma, Y. Suzuki, Y. Torii, T. Sugiura, T. Kuga, E. Hagley, and L. Deng, Science **286**, 2309 (1999).
[39] O. Zobay and G. Nikolopoulos, Phys. Rev. A **73**, 013620 (2006).
[40] L. Sadler, J. Higbie, S. Leslie, M. Vengalattore, and D. Stamper-Kurn, Phys. Rev. Lett. **98**, 110401 (2007).
[41] A. Öttl, S. Ritter, M. Köhl, and T. Esslinger, Phys. Rev. Lett. **95**, 090404 (2005).
[42] S. S. Hodgman, R. G. Dall, A. G. Manning, K. G. H. Baldwin, and A. G. Truscott, Science **331**, 1046 (2011).

[43] D. Schneble, Y. Torii, M. Boyd, E. W. Streed, D. E. Pritchard, and W. Ketterle, Science **300**, 475 (2003).
[44] L. F. Buchmann, G. M. Nikolopoulos, O. Zobay, and P. Lambropoulos, Phys. Rev. A **81**, 031606 (2010).
[45] W. RuGway, S. S. Hodgman, R. G. Dall, M. T. Johnsson, and A. G. Truscott, Phys. Rev. Lett. **107**, 075301 (2011).
[46] R. Bucker, J. Grond, S. Manz, T. Berrada, T. Betz, C. Koller, U. Hohenester, T. Schumm, A. Perrin, and J. Schmiedmayer, Nat. Phys. **7**, 608 (2011).
[47] M. Bonneau, J. Ruaudel, R. Lopes, J.-C. Jaskula, A. Aspect, D. Boiron, and C. I. Westbrook, Phys. Rev. A **87**, 061603 (2013).

I. SUPPLEMENTARY MATERIAL

Distribution of atoms in the xz plane The distribution of scattered atoms in the yz plane showed a vanishing population along the direction of the emission dipole (angles 0 and π in the Fig. 3 of the main text). In the xz plane on the other hand, the angular distribution is, as expected, uniform between the superradiant peaks, see Fig. S1. The signal is zero on one side of each superradiant peaks because the atomic cloud in the xz plane is off center with respect to the detector due to the photon recoil and the part of the distribution $k_x > 0.4\,k_{\rm rec}$ misses the detector, as shown in Fig. S2.

Calculation of the correlation functions The quantity actually displayed in Fig. 4 of the main text is not the correlation function as defined in Eq. 1, but the one defined by Eq. S1:

$$\tilde{g}^{(2)}(\Delta k_z)=\int_{\Omega_1}\mathrm{d}\Delta k_x\mathrm{d}\Delta k_y\int_{\Omega_V}\mathrm{d}^3\mathbf{k}\frac{\langle:\hat{n}(\mathbf{k})\hat{n}(\mathbf{k}+\Delta\mathbf{k}):\rangle}{\langle\hat{n}(\mathbf{k})\rangle\,\langle\hat{n}(\mathbf{k}+\Delta\mathbf{k})\rangle}$$
$$\tilde{g}^{(2)}(\Delta k_y)=\int_{\Omega_2}\mathrm{d}\Delta k_x\mathrm{d}\Delta k_z\int_{\Omega_V}\mathrm{d}^3\mathbf{k}\frac{\langle:\hat{n}(\mathbf{k})\hat{n}(\mathbf{k}+\Delta\mathbf{k}):\rangle}{\langle\hat{n}(\mathbf{k})\rangle\,\langle\hat{n}(\mathbf{k}+\Delta\mathbf{k})\rangle} \quad \text{(S1)}$$

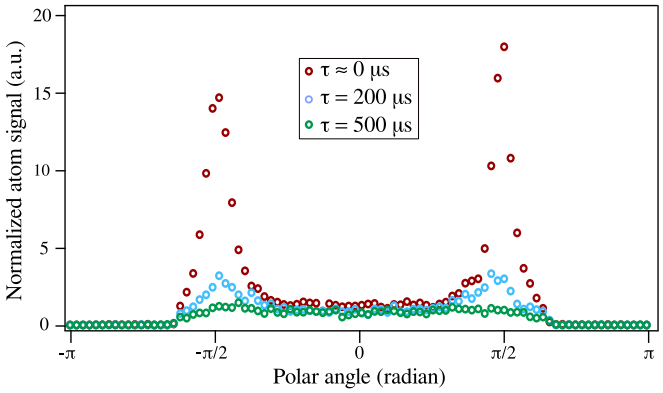

FIG. S1: (color online) Angular distribution of scattered atoms in the plane perpendicular to the emission dipole for different values of the delay τ before the excitation pulse. The data shown are the same as those discussed in the main text. Error bars not shown.

The volume Ω_1 is defined by the boundary conditions $|\Delta k_x| < 3\times10^{-2}\,k_{\rm rec}$, $|\Delta k_y| < 3\times10^{-2}\,k_{\rm rec}$ and Ω_2 by $|\Delta k_x| < 3\times10^{-2}\,k_{\rm rec}$, $|\Delta k_z| < 3\times10^{-3}\,k_{\rm rec}$. Integration in momentum space is performed over a specific volume Ω_V for each of the three cases showed in Fig. 4:

- superradiant peaks: $|k_x| < 0.5\,k_{\rm rec}$, $|k_y| < 0.5\,k_{\rm rec}$ and $|k_z| > 0.95\,k_{\rm rec}$;
- scattered sphere away from the superradiant peaks: $|k_z| < 0.92\,k_{\rm rec}$ and no constraint in the xy plane;
- stimulated Raman transfer: Ω_V is the volume centered on the cloud with a width along z of $0.1\,k_{\rm rec}$ and no constraint in the xy plane.

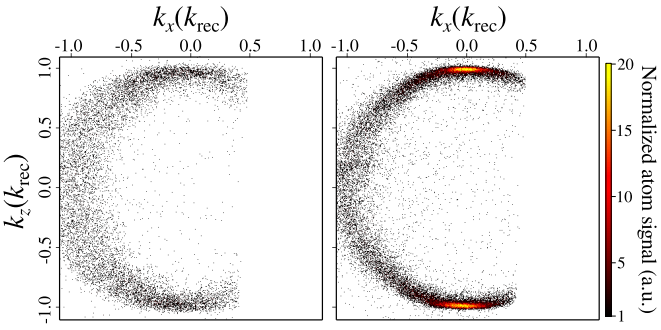

FIG. S2: (color online) Momentum distribution of scattered atoms in the plane perpendicular to the emission dipole. Both figures show the atom distribution in the xz plane, integrated between $k_y = \pm0.1\,k_{\rm rec}$ and summed over 100 shots. Left: Excitation laser applied 500 μs after the trap has been switched off. Only the radiation pattern for a y-polarized dipole is visible. Right: Excitation laser applied immediately after the trap has been switched off. Strong superradiance is visible in the vertical, endfire modes.

Widths of the superradiant peaks In order to obtain the widths of the superradiant peak, we first derive the contribution of ordinary spontaneous emission from the data with longest delay $\tau = 500\,\mu$s. These are well described by a pure spontaneous emission profile $\sin^2(\theta)$, where θ is the polar angle in the yz plane, as can be seen in Fig. S3 (green curve). Since the contribution of the spontaneous emission should be the same for all delays, we subtract this background from the atomic signal before fitting the distribution with a Lorentzian function. The sum of the background and the fit is also displayed in Fig. S3 (blue and red curves). The choice of a Lorentzian fitting function is empirical and we expect the exact shape of the superradiant contribution to be more complex [36]. From this fit we obtain half-widths at half-maximum of 0.14 and 0.25 rad for $\tau = 0$ and $200\,\mu$s, respectively.

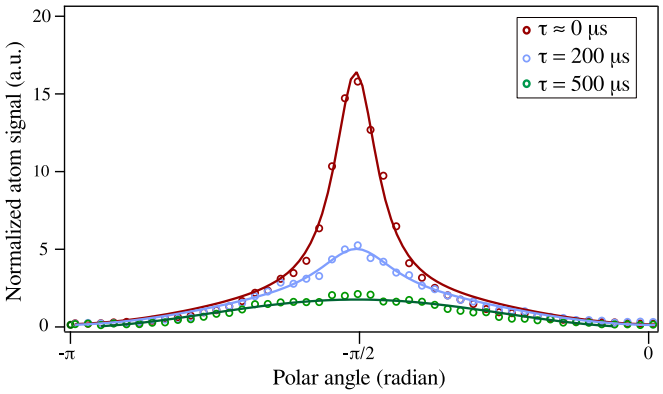

FIG. S3: (color online) Close up of the momentum distribution of scattered atoms around one superradiant peak in the plane of the emission dipole (yz plane). The data shown are the same as those discussed in the main text. Plain lines are fits to the data (see text for details). Error bars not shown.

Table I summarizes the various widths measured in this experiment. The first three lines refer to the widths of the observed atomic distribution in momentum space. The "BEC" entry corresponds to the configuration in which the $m = 0$ sublevel of the 2^3S_1 state was populated by stimulated Raman transfer (see main text).

TABLE I: Half-widths at half-maximum of the momentum distribution and correlation function in units of k_{rec}. The number in parenthesis denotes the uncertainty on the last digit.

Configuration	vertical	horizontal
BEC density	0.039(1)	0.190(2)
Superradiance density, $\tau = 0$	0.014(2)	0.14(2)
Superradiance density, $\tau = 200$ μs	0.032(2)	0.27(2)
Superradiance correlation, $\tau = 0$	0.021(2)	0.15(1)
Scattered sphere correlation, $\tau = 0$	0.014(2)	0.12(2)